CAUCHY – Jurnal Matematika Murni dan Aplikasi
Volume 11 (1) (2026), Pages 152-165
p-ISSN: 2086-0382; e-ISSN: 2477-3344

Implementation of DenseNet121 Based on Convolutional Neural Network with Geometric Augmentation for Breast Cancer Histopathology Image Classification

Nabilah Evi Ariani*, Sugiyarto Surono, and Aris Thobirin

Departemen of Mathematics, Ahmad Dahlan University, Yogyakarta, Indonesia

Abstract

This study evaluates the performance of the DenseNet121 architecture for binary classification of breast cancer histopathological images using the BreakHis dataset. The model employs ImageNet pre-trained weights, fine-tuning, and geometric data augmentation to improve feature learning and generalization. To obtain more reliable results, three optimization algorithms (Adam, AdamW, and RMSprop) were evaluated through repeated experiments, and performance was reported using mean and standard deviation of test metrics. The experimental results demonstrate that DenseNet121 achieves consistently high classification performance across different optimizers, with the Adam optimizer showing the most stable results. These findings indicate that DenseNet121 combined with data augmentation provides an effective and robust approach for histopathological image classification while emphasizing the importance of repeated evaluation for reliable performance assessment.

Keywords: Adam; AdamW; RMSprop; Breast Cancer; DenseNet121; Histopathology; Image Classification

1 Introduction

Advances in artificial intelligence, especially driven by deep learning methods, have had a significant impact on digital image analysis in various sectors in recent years [1][2][3]. Convolutional Neural Network (CNN) has become one of the leading architectural approaches due to its ability to automatically extract texture and spatial features without the need for manual extraction [4]. The use of CNNs is now quite widespread in industry, agriculture, and various pattern recognition systems due to their ability to recognize visual structures efficiently [5][6][7][8], making it the leading model in image classification tasks that require accurate and consistent analysis [9][10].

CNNs are effective, but their performance relies strongly on the robustness and completeness of the training data [11][12]. Small or highly diverse datasets often result in overfitting, especially if there are differences in lighting, color, or resolution [13][14]. To address this issue, data augmentation techniques are applied to increase data variation through geometric transformations such as rotation, flipping, zoom, translation, and contrast adjustment [15][16][17], which have been shown to improve model generalization [18][15]. In addition, augmentation methods based on generative models such as GAN and diffusion models have begun to be applied to create

*Corresponding author. E-mail: 2200015034@webmail.uad.ac.id

Submitted: December 05, 2025 Reviewed: December 17, 2025 Accepted: January 09, 2026
DOI: https://doi.org/10.18860/cauchy.v11i1.37896

synthetic images similar to the original data [19][20]. Transfer learning and fine-tuning of pre-trained models such as VGG, ResNet, EfficientNet, and DenseNet are often used to improve efficiency on limited datasets [21][22]. DenseNet121 stands out from the above models due to its dense connectivity, which enables feature reuse and stable gradient flow [23][24].

Previous research, including the study by Xiao et al. (2024), shows that CNNs can achieve high accuracy in breast cancer histopathology images by utilizing the BreakHis dataset [25]. However, several studies report that model performance can vary across different data splits, and high accuracy values may not always reflect performance stability. These findings indicate the importance of robust evaluation protocols when assessing CNN-based models for medical image classification.

Motivated by these observations, this study investigates the performance stability of DenseNet121 under different optimizer configurations combined with geometric data augmentation strategies. The BreakHis dataset, consisting of approximately 7,909 benign and malignant histopathology images, is employed as a benchmark dataset. Rather than proposing a new architecture, this work focuses on analyzing how optimizer choice influences classification performance and result variability under identical training conditions.

The main contribution of this study is a comparative evaluation of commonly used optimizers on a DenseNet121 architecture for breast cancer histopathology image classification. All experiments are conducted using identical data splits, augmentation strategies, and network configurations, with model performance reported as mean ± standard deviation across repeated runs. This analysis provides empirical insights into optimizer stability and performance variability, contributing to more reliable evaluation practices in deep learning-based medical image classification.

2 Methods

This study implements the DenseNet121 architecture as the main model for classifying breast cancer histopathology images, with a training process that utilizes Adam, AdamW, and RMSprop optimizations together with a Binary Cross-Entropy objective function. The complete flowchart of the research stages is shown in the following flowchart.

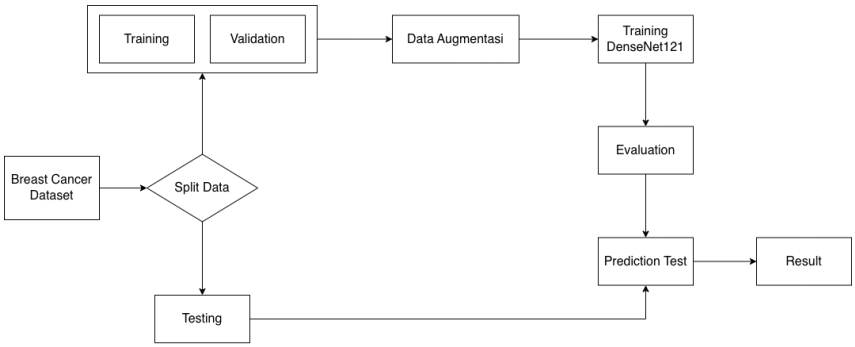

Figure 1: Research Flowchart

Fig. 1 shows the main stages of the research, starting from the division of the dataset into subsets for training, validation, and testing. Afterward, the training portion goes through a data-augmentation procedure to increase image diversity before being used in model training. The pretrained DenseNet121 is used as a feature extractor, then several classification layers are added before the training process. The final stage involves model evaluation and testing to assess overall classification performance.

2.1 Preprocessing

At this stage, all images undergo an initial preprocessing step to ensure a uniform data format prior to model training. Each image is resized to a spatial resolution of 224 × 224 pixels in order to match the standard input requirement of DenseNet121. This resizing process helps maintain consistency across the dataset while preserving essential spatial features relevant for classification. After resizing, the images are transformed into RGB format to construct three-channel inputs compatible with convolutional neural networks pre-trained on large-scale image datasets. This representation enables the network to effectively capture color-based and textural information from histopathological images. Subsequently, the dataset is divided into three subsets consisting of training, validation, and testing data. An 80%, 10%, 10% split is employed to ensure sufficient data for model learning while maintaining independent subsets for hyperparameter tuning and unbiased performance evaluation.

To increase data variety and minimize the likelihood of overfitting, the present work applied geometric data augmentation to histopathological images. The augmentation technique was applied randomly to each training batch to generate spatial variation without altering the original tissue structure.

The augmentations used include a rotation of 20°, horizontal and vertical translations of 10% each, a shear of 10%, a zoom of 10%, and a horizontal flip. This combination of transformations simulates variations in microscope scanning conditions so that the model receives a broader range of training samples and is able to learn network patterns more robustly.

2.2 Model Architecture

The model architecture in this study was built using DenseNet121 as the main feature extractor. DenseNet utilizes a dense connectivity mechanism, where each layer receives features from all previous layers.

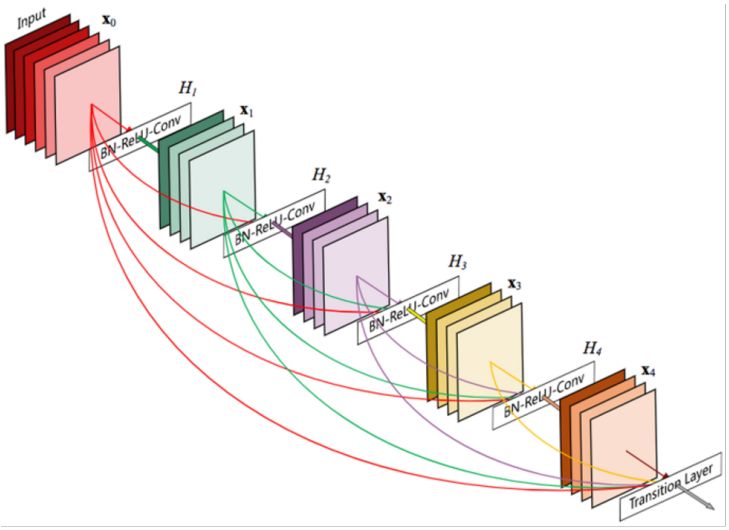

Figure 2: DenseNet Architecture

Fig. 2 shows an illustration of the general architecture of DenseNet, where every layer within the network is directly connected to all previous layers. This *dense connectivity* mechanism allows for a more stable gradient flow and more effective *feature reuse* [24].

Mathematically, this mechanism can be expressed in Eq. (1):

$$x_\ell = H_\ell\left([x_0, x_1, \ldots, x_{\ell-1}]\right), \tag{1}$$

in which x_ℓ represents the result produced by layer $_\ell$, $H_\ell(\cdot)$ is a composite operation (BatchNorm, ReLU, and Convolution), and $[\cdot]$ denotes the concatenation operation [24]. This approach enables

more stable gradient flow and more effective feature utilization.

The model uses pre-trained ImageNet weights with the setting `include_top = false` so that the model's built-in classification part is removed. To improve adaptability to histopathology datasets, only the last 30 layers are fine-tuned, while the initial layers are frozen to keep the basic features stable.

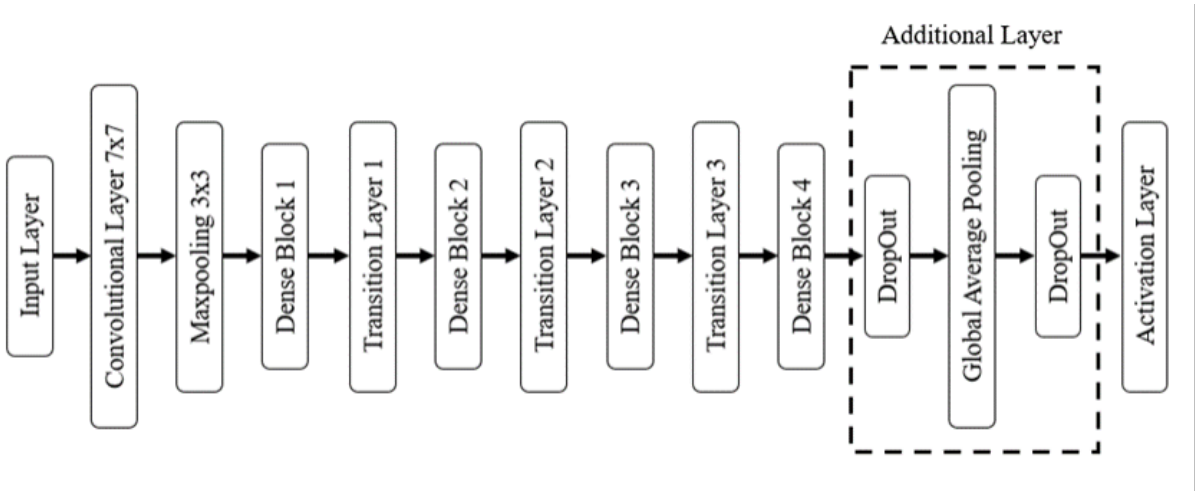

Figure 3: DenseNet121 Architecture

The complete architecture of DenseNet121 used in this study is presented in the Fig. 3. The diagram depicts the arrangement of dense blocks, transition layers, and additional layers (Global Average Pooling, Dense, and Dropout) applied at the end to support the binary classification process [24].

The output of DenseNet121 is a $7 \times 7 \times 1024$ tensor, which is then summarized using the Global Average Pooling (GAP) operation to convert spatial features into a single representative average value for each channel. GAP is used to reduce feature dimensions while preserving the core representation of each channel. It is more efficient than a fully connected layer and helps minimize the likelihood of overfitting.

After the pooling process, a fully connected layer containing 256 neurons with a ReLU function is added to produce a non-linear representation, followed by a dropout component set to 0.5 as a regularization mechanism. The final layer consists of two neurons activated with a sigmoid function to generate probability outputs for the two classes (benign and malignant).

The complete architectural structure is presented in Table 1.

Table 1: Model Architecture

Layer	Parameters
Base Model	DenseNet121 (ImageNet, include_top=False)
GlobalAveragePooling2D	Output vector of size 1024
Dense	256 units, activation = ReLU
Dropout	rate = 0.5
Dense (Output)	1 unit, activation = Sigmoid

2.3 Training Procedure

All experiments employed the same network architecture and training configuration, with the optimizer serving as the main variable under investigation. Adam, AdamW, and RMSprop were evaluated using identical hyperparameter settings. Training was performed for 20 epochs with a batch size of 32, and a ReduceLROnPlateau scheduler was applied to enhance training stability by decreasing the learning rate by a factor of 0.5 when validation loss showed no improvement

over five consecutive epochs. This design enables a controlled and fair comparison of optimizer performance for the binary classification task.

This research makes use of the Binary Cross-Entropy (BCE) loss, a function frequently applied in tasks involving two-class classification. Mathematically, BCE is expressed in Equation 2:

$$\mathcal{L}_{\text{BCE}}(y, \hat{y}) = -\left(y \log(\hat{y}) + (1 - y) \log(1 - \hat{y})\right). \tag{2}$$

Here, $y, \hat{y} \in \{0, 1\}$, where $\hat{y}$ denotes the predicted probability and y represents the ground truth label. This formulation corresponds to the Binary Cross-Entropy loss computed for an individual sample. During training, the overall loss is obtained by averaging the sample BCE over the mini batch [26].

To enhance the model's ability to adapt to histopathological imaging characteristics, approximately 30 layers of DenseNet121 were fine-tuned, while the initial layers were frozen to retain the basic features of pretrained ImageNet. The training process was conducted using augmented data to enrich sample variation and help prevent the risk of overfitting.

The complete training hyperparameter configuration is presented in Table 2.

Table 2: Training Hyperparameters

Parameter	**Value**
Optimizer	Adam, AdamW dan RMSprop
Learning rate (initial)	0.0001
Weight decay	0.00001
Batch size	32
Epochs	20
Loss function	Binary Cross-Entropy
Learning rate scheduler	ReduceLROnPlateau
Fine-tuned layers	Last 30 layers of DenseNet121

2.4 Evaluation Metrics

To assess how well the model performs in breast cancer two-class classification, this study uses several evaluation metrics commonly applied within computer vision research, namely accuracy, precision, recall, and the F1-score. Each metric is derived using prediction values obtained through the confusion matrix, which consists of TP (True Positive), TN (True Negative), FP (False Positive), and FN (False Negative) [27]. The definition of each metric is stated as follows.

Accuracy measures the share of correctly predicted outcomes against the entire sample and is formally expressed in Eq. (3).

$$\text{Accuracy} = \frac{TP + TN}{TP + TN + FP + FN}. \tag{3}$$

Precision measures the accuracy of the model in predicting positive classes, or the proportion of correct positive predictions. The precision metric is defined in Eq. (4).

$$\text{Precision} = \frac{TP}{TP + FP}. \tag{4}$$

Recall assesses the model's capacity to recognize all actual positive cases, which is the fraction of true positive samples successfully detected. Recall is formulated in Eq. (5).

$$\text{Recall} = \frac{TP}{TP + FN}. \tag{5}$$

The F1-score is the harmonic mean between precision and recall, which provides a more balanced measure of performance, especially in conditions of imbalanced data. The F1-score is calculated as shown in Eq. (6).

$$\text{F1-Score} = 2 \cdot \frac{\text{Precision} \times \text{Recall}}{\text{Precision} + \text{Recall}} \tag{6}$$

3 Results and Discussion

This section presents the experimental results of the proposed deep learning approach. The discussion covers the dataset, preprocessing, data augmentation, and model architecture. Model performance is evaluated through repeated test experiments using mean and standard deviation to assess prediction stability across optimizers.

3.1 Dataset

The dataset consists of 7,909 breast cancer histopathological images, including 2,480 benign and 5,429 malignant samples. The DenseNet121 model is implemented using the Keras Functional API, and the data are partitioned into training, validation, and test sets using a stratified 80%, 10%, and 10% split. The training and validation sets are used for model learning, while the test set is reserved for evaluation and contains 791 images (248 benign and 543 malignant). The same data split is maintained across all experiments, and the reported results represent the mean and standard deviation obtained from repeated runs.

3.2 Augmentation

The training data is subjected to a set of augmentation operations using ImageDataGenerator. These augmentation steps involve applying rotation, horizontal and vertical shifts, shear transformation, zooming, horizontal flipping, and fill-mode adjustments. The detailed augmentation settings are provided in Table 3.

Table 3: Data Augmentation Parameters

Function	Parameters
Rotation_range	20
Width_shift_range	0.10
Height_shift_range	0.10
Shear_range	0.10
Zoom_range	0.10
Horizontal_flip	'True'
Fill_mode	'nearest'

Table 3 shows the data augmentation parameters used to enrich image variation in the training data. This approach enables the model to achieve more stable learning and lowers the likelihood of overfitting.

3.3 Training Model Architecture

Training employed a preinitialized DenseNet121 model trained on ImageNet. Its dense connectivity enables efficient feature reuse and robust extraction of complex patterns, making it suitable for histopathological image analysis without training a network from scratch. The complete architecture can be seen in Table 4.

Table 4: DenseNet121 Layer Summary

Layers	Parameters
GlobalAveragePooling2D	1024-feature vector
Dense	256, activation = 'relu'
Dropout	0.5
Output Dense	1, activation = 'sigmoid'
Label Encoding	Binary (0/1)

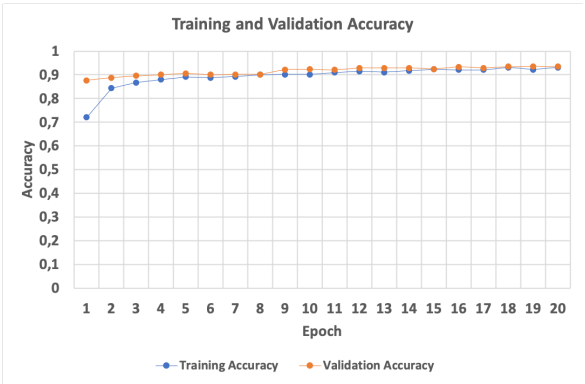

(a) Accuracy Adam 1

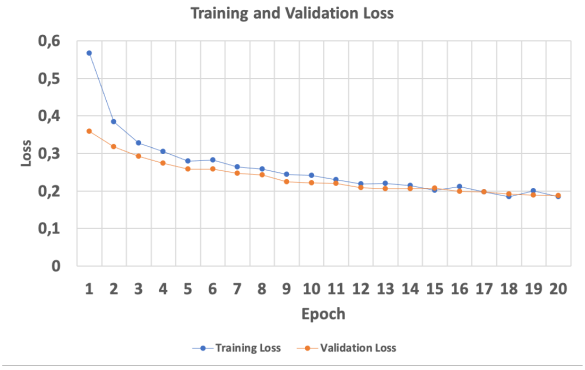

(b) Loss Adam 1

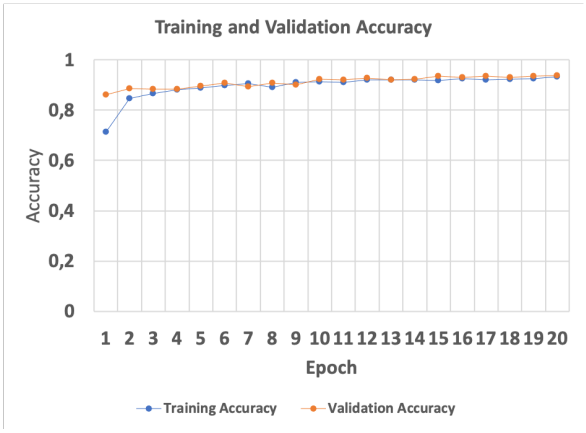

(c) Accuracy Adam 2

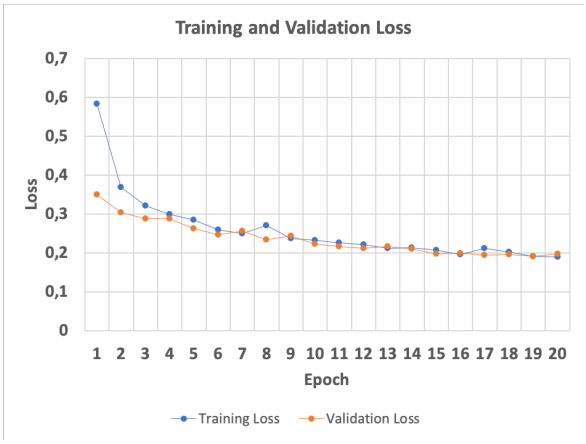

(d) Loss Adam 2

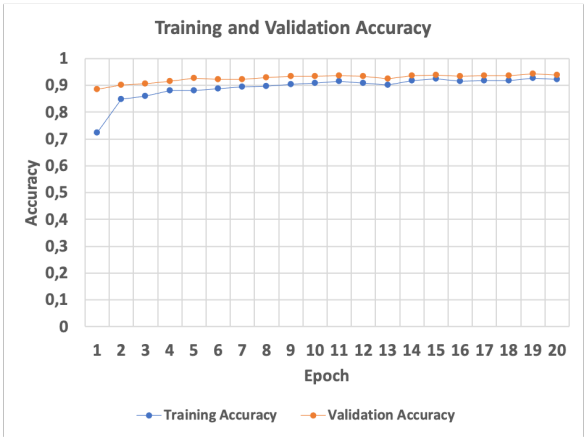

(e) Accuracy Adam 3

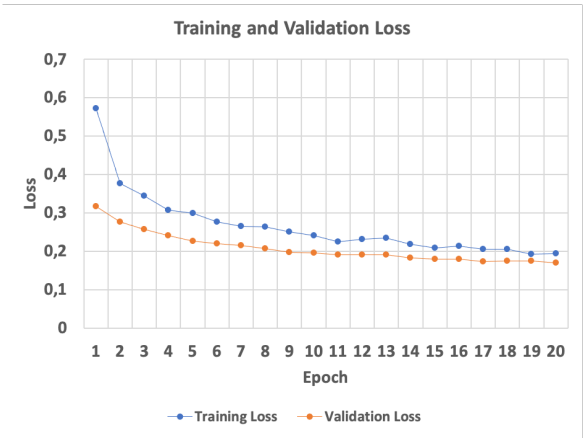

(f) Loss Adam 3

Figure 4: Training and validation performance of DenseNet121 using Adam optimizer across three runs.

The model training phase used 20 epochs and consisted of 198 iterations per epoch. The loss function applied was binary cross-entropy. To analyze the impact of optimization strategies, three optimizers (Adam, AdamW, and RMSprop) were evaluated under identical training settings (learning rate = 0.0001). Each configuration was trained three times from scratch to reduce randomness, and performance is reported as mean ± standard deviation.

Fig. 4 presents the training and validation accuracy and loss curves of the DenseNet121 model trained with the Adam optimizer across three experimental runs. The accuracy increases steadily while the loss values decrease throughout training, indicating effective learning behavior. Minor variations appear during the early epochs; however, the overall trends remain consistent,

suggesting stable optimization and satisfactory generalization without evident overfitting.

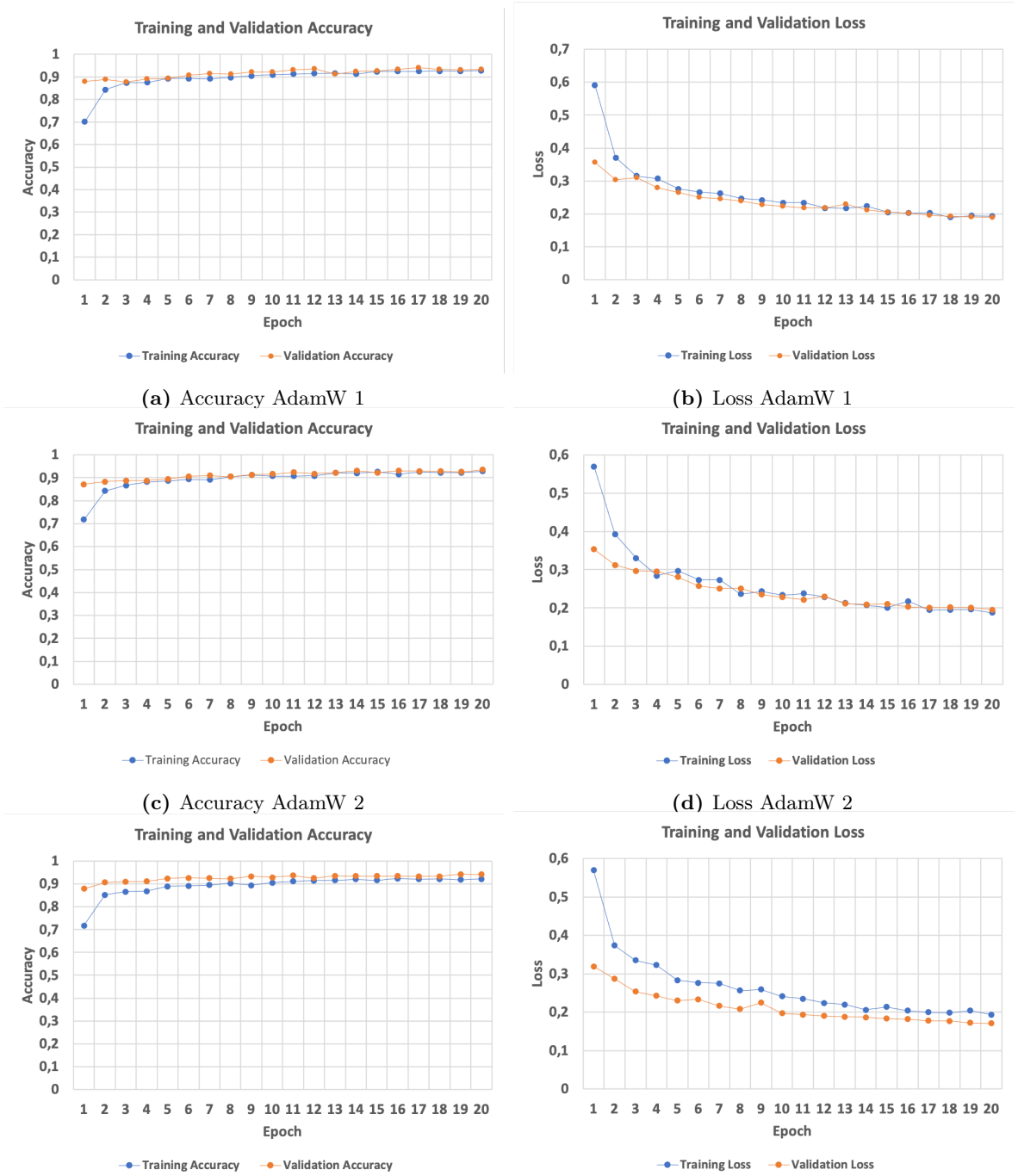

(a) Accuracy AdamW 1 **(b)** Loss AdamW 1

(c) Accuracy AdamW 2 **(d)** Loss AdamW 2

(e) Accuracy AdamW 3 **(f)** Loss AdamW 3

Figure 5: Training and validation performance of DenseNet121 using AdamW optimizer across three runs.

Fig. 5 illustrates the training and validation accuracy and loss curves of the DenseNet121 model trained using the AdamW optimizer across three repeated experiments. The accuracy consistently improves throughout training, while the loss values decrease steadily, indicating effective optimization. Minor variations are observed during the early epochs. However, the overall convergence remains stable under fixed hyperparameter settings. The smooth loss reduction achieved with AdamW suggests improved regularization, and the close alignment between training and validation trends indicates satisfactory generalization without evident overfitting.

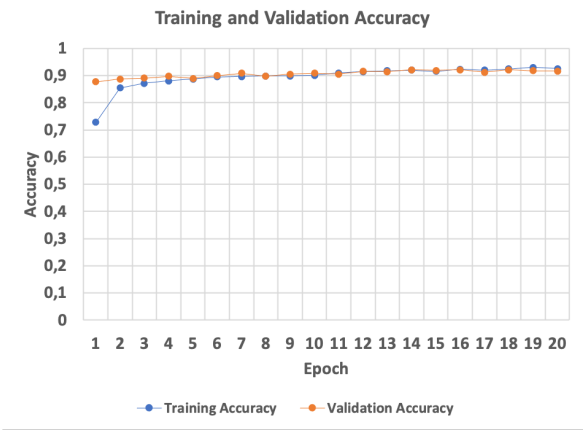

(a) Accuracy RMSprop 1

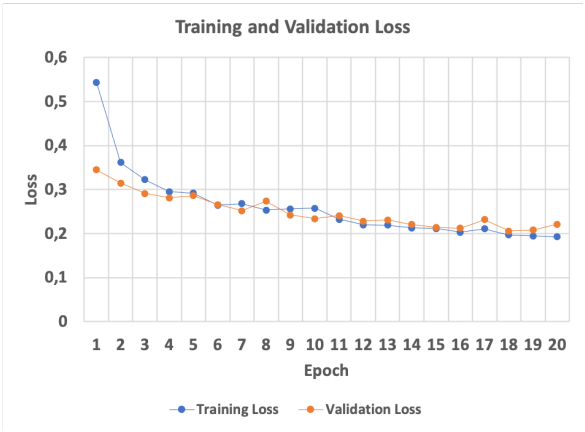

(b) Loss RMSprop 1

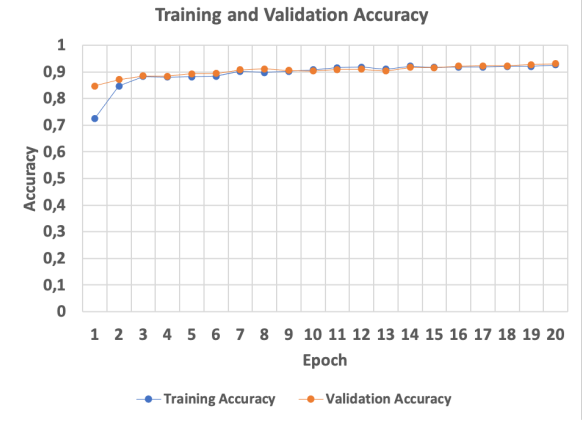

(c) Accuracy RMSprop 2

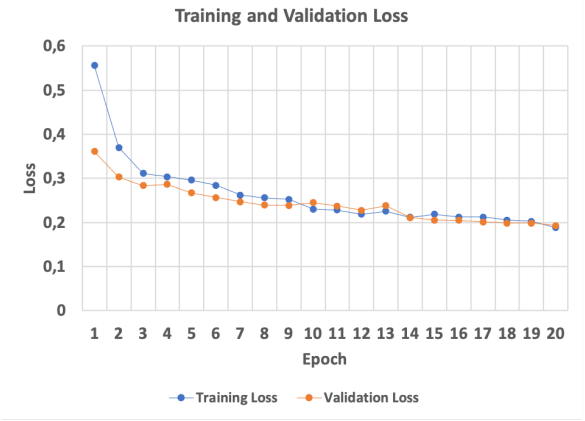

(d) Loss RMSprop 2

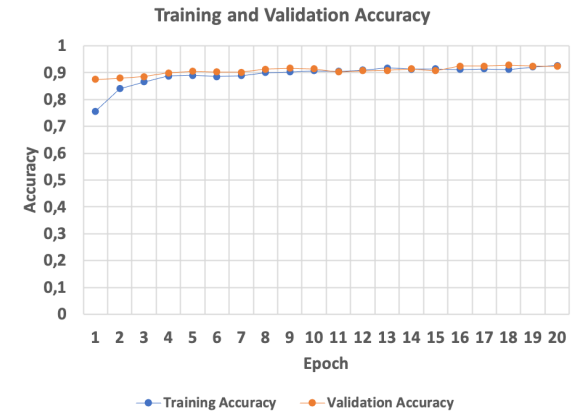

(e) Accuracy RMSprop 3

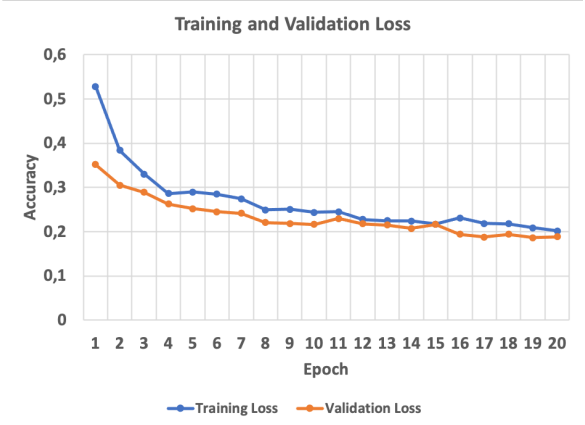

(f) Loss RMSprop 3

Figure 6: Training and validation performance of DenseNet121 using RMSprop optimizer across three runs.

Fig. 6 shows the training and validation accuracy and loss curves of the DenseNet121 model optimized using the RMSprop algorithm across three training runs. The accuracy curves consistently increase and stabilize as the number of epochs progresses, while the loss curves gradually decrease, indicating effective learning and convergence. Across all runs, the training and validation curves remain closely aligned, suggesting that the model generalizes well without exhibiting severe overfitting. Minor variations observed between runs mainly occur in the early epochs and do not significantly affect the overall training behavior, demonstrating the stability

of RMSprop under identical training settings.

Table 5: Training and Validation Performance of DenseNet121 Across Optimizers (Mean ± Std)

Optimizer	Train Acc	Val Acc	Train Loss	Val Loss
Adam	0.9286 ± 0.0064	0.9368 ± 0.0025	0.1890 ± 0.0053	0.1847 ± 0.0132
AdamW	0.9260 ± 0.0027	0.9368 ± 0.0043	0.1914 ± 0.0032	0.1851 ± 0.0124
RMSprop	0.9260 ± 0.0007	0.9233 ± 0.0071	0.1943 ± 0.0067	0.2009 ± 0.0151

Table 5 presents the average training and validation performance of DenseNet121 across different optimizers. The results show that all configurations converge consistently with relatively small variations, indicating stable training behavior. Among the evaluated optimizers, Adam exhibit more reliable validation performance compared to RMSprop, which shows slightly higher variability.

3.4 Model Prediction Results

This subsection presents the prediction performance of the DenseNet121 model evaluated on the test dataset. To assess the stability and generalization capability of the model, three independent training runs were conducted for each optimizer configuration. Model performance was measured using accuracy, precision, recall, and F1-score, which were then summarized using the mean and standard deviation to capture both central tendency and variability across runs. Precision, recall, and F1-score are reported using weighted averaging to account for class imbalance in the dataset. In this study, the malignant class is treated as the positive class (label 1), while benign samples correspond to the negative class (label 0). Accordingly, recall reflects the model's ability to correctly identify malignant cases, whereas precision indicates the reliability of malignant predictions.

The mean and standard deviation of each evaluation metric are computed using Eq. (7) and Eq. (8).

$$\bar{x} = \frac{1}{n}\sum_{i=1}^{n} x_i \tag{7}$$

$$\sigma = \sqrt{\frac{1}{n-1}\sum_{i=1}^{n}(x_i - \bar{x})^2} \tag{8}$$

Table 6: Prediction performance of DenseNet121 using Adam optimizer (mean ± standard deviation)

Optimizer	Accuracy (%)	Precision (%)	Recall (%)	F1-score (%)
Adam	93.63 ± 0.80	93.63 ± 0.82	93.63 ± 0.80	93.61 ± 0.84

Table 6 summarizes the prediction performance of the DenseNet121 model on the test dataset using the Adam optimizer. The results indicate consistently high accuracy, precision, recall, and F1-score values across repeated runs, with relatively small standard deviations. This suggests that the model achieves stable and reliable predictive performance when optimized using Adam, while maintaining good generalization on unseen data.

Table 7: Prediction performance of DenseNet121 using AdamW optimizer (mean ± standard deviation)

Optimizer	Accuracy (%)	Precision (%)	Recall (%)	F1-score (%)
AdamW	92.88 ± 0.89	92.85 ± 0.90	92.88 ± 0.89	92.80 ± 0.90

Table 7 summarizes the prediction performance of the DenseNet121 model optimized using AdamW. The results indicate stable performance across three independent runs, as reflected by the relatively small standard deviations. Overall, AdamW achieves competitive accuracy and

balanced precision–recall values on the test dataset, demonstrating consistent generalization capability.

Table 8: Prediction performance of DenseNet121 using RMSprop optimizer (mean ± standard deviation)

Optimizer	**Accuracy (%)**	**Precision (%)**	**Recall (%)**	**F1-score (%)**
RMSprop	92.25 ± 1.18	92.33 ± 0.98	92.25 ± 1.18	92.11 ± 1.32

Table 8 presents the prediction performance of the DenseNet121 model optimized using RMSprop. The results show slightly higher variability across runs compared to Adam and AdamW, as indicated by larger standard deviations. Nevertheless, RMSprop maintains competitive accuracy and balanced precision, recall values on the test dataset, indicating stable but less consistent performance under repeated training.

Based on the results presented in Table 6–Table 8, the DenseNet121 model demonstrates strong and consistent prediction performance across all evaluated optimization strategies. Among the three optimizers, Adam achieves the highest overall accuracy and F1-score with the smallest standard deviation, indicating superior stability and reliable generalization on the test dataset. AdamW also shows competitive performance with balanced precision and recall values, suggesting its effectiveness in maintaining robust predictions while incorporating weight decay regularization. In contrast, RMSprop exhibits slightly higher variability across runs, as reflected by larger standard deviations, although its overall accuracy and class-wise performance remain comparable. These findings indicate that while all optimizers are capable of producing satisfactory results, Adam provides the most stable and consistent performance for the DenseNet121 model on the BreakHis dataset.

4 Conclusion

This study evaluated the performance of the DenseNet121 model for breast cancer histopathology image classification using the BreakHis dataset under repeated experimental settings. Three optimizers (Adam, AdamW, and RMSprop) were assessed using identical hyperparameters and geometric data augmentation, with each configuration trained three times to reduce randomness. The results demonstrate that DenseNet121 achieves consistently high predictive performance, as reflected by stable training validation curves and competitive test accuracy, precision, recall, and F1-score values. Among the evaluated optimizers, Adam showed the most stable performance with the highest average metrics and the lowest variability across runs, while AdamW provided comparable results and RMSprop exhibited slightly higher variation but remained competitive.

These findings indicate that DenseNet121 combined with geometric data augmentation is an effective and reliable approach for histopathological image classification on limited medical datasets. The use of repeated experiments and statistical evaluation strengthens the robustness of the performance assessment and avoids overclaiming generalization capability. For further research, it is recommended to use a larger and more diverse dataset, as well as explore other architectures or advanced data balancing techniques to improve model stability during the classification process. This study is expected to contribute to computer-aided diagnosis for early detection of breast cancer.

CRediT Authorship Contribution Statement

Nabilah Evi Ariani: Conceptualization, Methodology, Software, Data curation, Formal analysis, Visualization, Writing – original draft, Writing & editing. **Sugiyarto Surono**: Supervision, Validation, Methodology consultation, Review. **Aris Thobirin**: Supervision, Resources, Project administration, Review.

Declaration of Generative AI and AI-assisted technologies

This study made limited use of Generative AI tools (ChatGPT) for linguistic editing and clarity enhancement. The AI tools were not involved in generating ideas, performing experiments, analyzing data, interpreting findings, or drawing scientific conclusions. All substantive contributions, including the methodology, analysis, and results, were developed exclusively by the authors.

Declaration of Competing Interest

The authors state that no conflicts of interest are present, whether financial, personal, or professional, that might have affected the research, analysis, or conclusions presented in this paper.

Funding and Acknowledgments

The authors wish to convey their heartfelt appreciation to the academic supervisors for providing ongoing guidance, constructive input, and meaningful insights during the entire course of this research. Appreciation is also extended to the Laboratory of the Mathematics Department, Universitas Ahmad Dahlan, for providing essential facilities and technical support that greatly contributed to the completion of this study.

Data and Code Availability

The dataset employed in this research can be openly accessed on the Kaggle platform and can be obtained through the original source repository. The code developed for model training, evaluation, and analysis can be requested from the corresponding author, subject to reasonable inquiry, as it contains project-specific configurations and internal processing scripts.

References

[1] T. Huang, X. Huang, and H. Yin, "Deep learning methods for improving the accuracy and efficiency of pathological image analysis," *Scientific Progress*, vol. 108, no. 1, pp. 1–34, 2025. [Online]. Available: https://doi.org/10.1177/00368504241306830

[2] M. Trigka and E. Dritsas, "A comprehensive survey of deep learning approaches in image processing," *Sensors*, Jan. 2025. [Online]. Available: https://doi.org/10.3390/s25020531

[3] J. Wang, S. Wang, and Y. Zhang, "Deep learning on medical image analysis," *Computational Intelligence and Technology*, Feb. 2025. [Online]. Available: https://doi.org/10.1049/cit2.12356

[4] A. E. Minarno, M. Fadhlan, Y. Munarko, and R. Chandranegara. Classification of dermoscopic images using cnn-svm. https://www.joiv.org/index.php/joiv. Accessed: 2025-01-01.

[5] G. Li *et al.*, "Practices and applications of convolutional neural network-based computer vision systems in animal farming: A review," *Sensors*, Feb. 2021. [Online]. Available: https://doi.org/10.3390/s21041492

[6] M. E. Sakka, M. Ivanovici, L. Chaari, and J. Mothe, "A review of cnn applications in smart agriculture using multimodal data," *Sensors*, Jan. 2025. [Online]. Available: https://doi.org/10.3390/s25020472

[7] R. Raj and A. Kos, "An extensive study of convolutional neural networks: Applications in computer vision for improved robotics perceptions," *Sensors*, Feb. 2025. [Online]. Available: https://doi.org/10.3390/s25041033

[8] X. Zhao, W. Tang, Q. Liu, H. Cao, and F. Chen, "Impact of agricultural industry transformation based on deep learning model evaluation and metaheuristic algorithms under dual carbon strategy," *Scientific Reports*, vol. 15, no. 1, Dec. 2025. [Online]. Available: https://doi.org/10.1038/s41598-025-14073-1

[9] L. Lahouaoui, D. Abdelhak, B. Abderrahmane, and M. Toufik, "Image classification using a fully convolutional neural network cnn," *Mathematical Modelling of Engineering Problems*, vol. 9, no. 3, pp. 771–778, Jun. 2022. [Online]. Available: https://doi.org/10.18280/mmep.090325

[10] S. Dani, P. S. Hanwate, H. Panse, K. Chaudhari, and S. Kotwal. (2021) Survey on the use of cnn and deep learning in image classification. https://www.jetir.org. Accessed: 2025-01-01.

[11] J. Valente, J. António, C. Mora, and S. Jardim, "Developments in image processing using deep learning and reinforcement learning," *Journal of Imaging*, Oct. 2023. [Online]. Available: https://doi.org/10.3390/jimaging9100207

[12] R. B. S, P. K. N, S. S. M, A. Professor, and E. Dept. Brief study on convolutional neural networks. https://www.ijfmr.com. Accessed: 2025-01-01.

[13] A. Safonova, G. Ghazaryan, S. Stiller, M. Main-Knorn, C. Nendel, and M. Ryo, "Ten deep learning techniques to address small data problems with remote sensing," *International Journal of Applied Earth Observation and Geoinformation*, Dec. 2023. [Online]. Available: https://doi.org/10.1016/j.jag.2023.103569

[14] M. Xu *et al.*, "Embracing limited and imperfect training datasets: opportunities and challenges in plant disease recognition using deep learning," *Frontiers in Plant Science*, vol. 14, 2023. [Online]. Available: https://doi.org/10.3389/fpls.2023.1225409

[15] W. Zeng, "Image data augmentation techniques based on deep learning: A survey," *Mathematical Biosciences and Engineering*, 2024. [Online]. Available: https://doi.org/10.3934/mbe.2024272

[16] A. Tatar, M. Haghighi, and A. Zeinijahromi, "Experiments on image data augmentation techniques for geological rock type classification with convolutional neural networks," *Journal of Rock Mechanics and Geotechnical Engineering*, vol. 17, no. 1, pp. 106–125, Jan. 2025. [Online]. Available: https://doi.org/10.1016/j.jrmge.2024.02.015

[17] M. Das, M. Panda, and S. Dash, "Enhancing the power of cnn using data augmentation techniques for odia handwritten character recognition," *Advances in Multimedia*, vol. 2022, 2022. [Online]. Available: https://doi.org/10.1155/2022/6180701

[18] S. Kumar, P. Asiamah, O. Jolaoso, and U. Esiowu. (2025, Feb.) Enhancing image classification with augmentation: Data augmentation techniques for improved image classification. http://arxiv.org/abs/2502.18691. ArXiv preprint.

[19] R. Gulakala, B. Markert, and M. Stoffel, "Generative adversarial network based data augmentation for cnn based detection of covid-19," *Scientific Reports*, vol. 12, no. 1, Dec. 2022. [Online]. Available: https://doi.org/10.1038/s41598-022-23692-x

[20] T. Koenig, L. Cadau, F. Wagner, and M. Kley, "A generative adversarial network-based data augmentation approach with transient vibration data," in

Procedia Computer Science. Elsevier B.V., 2023, pp. 1340–1349. [Online]. Available: https://doi.org/10.1016/j.procs.2023.10.122

[21] H. S. ALGhafri and C. S. Lim, "Fine-tuning models for histopathological classification of colorectal cancer," *Diagnostics*, vol. 15, no. 15, p. 1947, Aug. 2025. [Online]. Available: https://doi.org/10.3390/diagnostics15151947

[22] A. R. Philip, "Fine-tuning depth analysis: Identifying the sweet spot for maximum accuracy in cnns," *International Journal of Scientific Research in Computer Science and Engineering*, vol. 13, no. 3, pp. 48–63, Jun. 2025. [Online]. Available: https://doi.org/10.26438/ijsrcse.v13i3.703

[23] N. Hasan, Y. Bao, A. Shawon, and Y. Huang, "Densenet convolutional neural networks application for predicting covid-19 using ct image," *SN Computer Science*, vol. 2, no. 5, Sep. 2021. [Online]. Available: https://doi.org/10.1007/s42979-021-00782-7

[24] S. Sabila. (2024, Jul.) Multiple brain tumor with modified densenet121 architecture using brain mri images. [Online]. Available: https://doi.org/10.21107/kursor.v12i3.379

[25] M. Xiao, Y. Li, X. Yan, M. Gao, and W. Wang. (2024, Apr.) Convolutional neural network classification of cancer cytopathology images: Taking breast cancer as an example. [Online]. Available: https://doi.org/10.48550/arXiv.2404.08279

[26] M. Yeung, E. Sala, C. Schönlieb, and L. Rundo, "Unified focal loss: Generalising dice and cross entropy-based losses to handle class imbalanced medical image segmentation," *Computerized Medical Imaging and Graphics*, 2021, preprint, arXiv:2102.04525v4. [Online]. Available: https://arxiv.org/abs/2102.04525

[27] N. A. Sovia, N. W. S. Wardhani, E. Sumarminingsih, and E. R. Shofa, "Enhancing image classification of cabbage plant diseases using a hybrid model convolutional neural network and xgboost," *CAUCHY: Jurnal Matematika Murni dan Aplikasi*, vol. 10, no. 1, pp. 278–289, Feb. 2025. [Online]. Available: https://doi.org/10.18860/ca.v10i1.30866